JOURNAL OF GUIDANCE, CONTROL, AND DYNAMICS
Vol. 46, No. 2, February 2023

# Engineering Notes

## Prescribed Performance-Based Fixed-Time Adaptive Control Allocation for Overactuated Spacecraft

Zeyu Kang,* Qiang Shen,† and Shufan Wu‡
*Shanghai Jiao Tong University, 200240 Shanghai, People's Republic of China*
and
Christopher J. Damaren§
*University of Toronto, Toronto, Ontario M3H 5T6, Canada*

https://doi.org/10.2514/1.G006915



### I. Introduction

AS ONE of the most important parts of a spacecraft completing its mission on orbit, attitude control has attracted a great deal of interest. In practice, considering the safety and reliability of the spacecraft, attitude control under a certain degree of redundancy has become a hot topic. Because redundant actuators are used in modern spacecraft, better control performance and more safety than that with three control actuators can be achieved [1].

In recent years, control allocation (CA) technology has been applied to manage the actuator redundancy of overactuated systems to distribute the desired high-level virtual/total control action to the available low-level actuators. In addition, the high-level controller and low-level CA can usually be designed separately [2–4]. The essence of the CA problem can be solved as an optimization problem. In [5], the sliding mode controller and static CA were constructed as a min-max optimization problem under actuator failure. In traditional static CA, the optimization is solved within any two consecutive sampling instances such that the first-order optimality set is always satisfied. However, this may not be achievable due to the limited capability of the onboard computer.

To avoid solving the optimization problem in each sampling period, an adaptive CA (ACA) was proposed in [6], which is a dynamic CA approach that constructs parameter adaptive laws to obtain asymptotic convergence to the first-order optimality set. Based on ACA, a control algorithm was designed in [7] for the motion tracking of a four-wheel ground vehicle and realizing optimal energy consumption. In [8], a near-optimal ACA scheme attitude controller was designed for overactuated spacecraft, where single-gimbal control moment gyros and reaction wheels are employed as actuators. However, the output saturation of the actuators was not considered in the CA problem, which may lead to control failure. Recently, a finite-time ACA (FT-ACA) was proposed in [9] to guarantee finite-time CA error convergence with actuator saturation. Compared with the ACA algorithm in [7,8], it improves the convergence speed of the allocation error. However, the settling time of the CA error relies explicitly on the initial condition of the system, leading to the limited application scope of the aforementioned results in FT-ACA, especially when information of initial states is unknown or unavailable. In addition, these aforementioned adaptive CA methods only focus on the steady-state performance of ACA, while the transient performance is ignored. To the best of our knowledge, designing an ACA approach with fixed-time allocation error convergence and prescribed transient performance guarantee is still an open problem.

In this paper, we consider the rest-to-rest attitude control problem for the overactuated spacecraft subject to actuator saturation limitations. To tackle this challenging problem, a two-level control structure consisting of a high-level controller and a low-level prescribed performance-based fixed-time ACA is proposed. First, different from the static CA problem in [6–8], which takes the CA error as the constraint, we configure the CA error in the objective function to avoid the problem that the CA cannot match when the control torque is excessive due to considering the actuator saturation constraint. Second, in contrast to the existing ACA approaches with asymptotic [6–8] or finite-time [9,10] CA error convergence, we formulate an appointed-time prescribed performance-based fixed-time adaptive control allocation (ATPP-FixTACA) that not only achieves fixed-time convergence of the ACA error but also guarantees appointed-time predefined ACA transient performance, resulting in improved convergence rate and better dynamic performance. Finally, we demonstrate the efficiency of the proposed CA approach through numerical simulation on a rigid spacecraft performing a rest-to-rest attitude maneuver.

The remainder of this paper is organized as follows. The dynamics and kinematics of overactuated spacecraft and CA problem are modeled in Sec. II. The problem to be solved in this paper is stated in Sec. III. The ATPP-FixTACA method considering actuator saturation constraint is designed to distribute the virtual torque to each actuator in Sec. IV. Simulation results under the high-level attitude controller and low-level CA methods are demonstrated in Sec. VI. Finally, conclusions are provided in Sec. VII.

### II. Preliminaries

#### A. Kinematics and Dynamics Equations

Let $\boldsymbol{Q} = [\boldsymbol{q}^T, q_0]^T \in \mathbb{R}^3 \times \mathbb{R}$ denote the unit-quaternion with respect to the inertial frame $\mathcal{I}$ expressed in the body frame $\mathcal{B}$. Define $\boldsymbol{Q}_d = [\boldsymbol{q}_d^T, q_{d0}]^T \in \mathbb{R}^3 \times \mathbb{R}$ as the desired attitude with inverse or conjugate denoted as $\boldsymbol{Q}_d^*$. As a result, the unit-quaternion error is computed as $\boldsymbol{Q}_e = \boldsymbol{Q}_d^* \otimes \boldsymbol{Q} = [\boldsymbol{q}_e^T, q_{e0}]^T \in \mathbb{R}^3 \times \mathbb{R}$, where $\otimes$ is the quaternion multiplication operator. In this paper, because we focus on rest-to-rest attitude maneuvers, the equation governing the attitude error kinematics is given by [11]

$$\dot{\boldsymbol{Q}}_e = \frac{1}{2}\boldsymbol{Q}_e \otimes \boldsymbol{\nu}(\boldsymbol{\omega}) = \frac{1}{2}\begin{bmatrix} \boldsymbol{S}(\boldsymbol{q}_e) + q_{e0}\boldsymbol{I}_3 \\ -\boldsymbol{q}_e^T \end{bmatrix}\boldsymbol{\omega} \tag{1}$$

where $\boldsymbol{\omega} \in \mathbb{R}^3$ is the angular velocity vector of the spacecraft, which is respect to the inertial frame $\mathcal{I}$ and expressed in the body frame $\mathcal{B}$; the function $\boldsymbol{\nu}$: $\mathbb{R}^3 \to \mathbb{R}^4$ is defined as $\boldsymbol{\nu}(\boldsymbol{\omega}) = [\boldsymbol{\omega}^T, 0]^T$; and the operation

Received 25 April 2022; revision received 13 August 2022; accepted for publication 14 October 2022; published online 30 November 2022. 

*Ph.D. Student, School of Aeronautics and Astronautics; kangzeyu@sjtu.edu.cn.
†Associate Professor, School of Aeronautics and Astronautics; qiangshen@sjtu.edu.cn. Member AIAA.
‡Professor, School of Aeronautics and Astronautics; shufan.wu@sjtu.edu.cn. Associate Fellow AIAA.
§Professor, Institute for Aerospace Studies; damaren@utias.utoronto.ca. Associate Fellow AIAA.

$$S(\boldsymbol{x}) = \begin{bmatrix} 0 & -x_3 & x_2 \\ x_3 & 0 & -x_1 \\ -x_2 & x_1 & 0 \end{bmatrix} \in \mathbb{R}^{3\times 3} \tag{2}$$

is to generate a skew-symmetric matrix for any vector $\boldsymbol{x} \in \mathbb{R}^3$.

The attitude dynamics of the nonrigid spacecraft [5,12] is defined by the following rotational motion equation:

$$\boldsymbol{J}\dot{\boldsymbol{\omega}} = -\boldsymbol{S}(\omega)\boldsymbol{J}\boldsymbol{\omega} + \boldsymbol{D}\boldsymbol{\tau} \tag{3}$$

where $\boldsymbol{J} \in \mathbb{R}^{3\times 3}$ denotes the inertia matrix of the spacecraft, $\boldsymbol{D} \in \mathbb{R}^{3\times N}$ is the installation matrix, $N > 3$ represents the number of actuators configured for the overactuated spacecraft, and $\boldsymbol{\tau} \in \mathbb{R}^N$ is the output torque of the actuators.

### B. Control Allocation Problem

Due to the physical limitations of spacecraft actuators, the output saturation of actuators is considered in the CA problem. Without losing generality, it is assumed that each actuator has the different output saturation value, i.e., $\tau_{i,\min} \le \tau_i \le \tau_{i,\max}$, $i = 1, 2, \ldots, N$, where $\tau_{i,\min}$ and $\tau_{i,\max}$ represent the positive constants of the upper and lower limits of output saturation of each actuator, respectively. Then, considering that the spacecraft is equipped with $N > 3$ actuators, the static CA problem in this work is expressed as

$$\begin{aligned} \min_{\boldsymbol{\tau}} \quad & J_e = \tfrac{1}{2}(\boldsymbol{D}\boldsymbol{\tau} - \boldsymbol{u})^T\boldsymbol{H}(\boldsymbol{D}\boldsymbol{\tau} - \boldsymbol{u}) + \tfrac{1}{2}\boldsymbol{\tau}^T\boldsymbol{M}\boldsymbol{\tau} \\ \text{s.t.} \quad & \tau_{i,\min} \le \tau_i \le \tau_{i,\max}, \ i = 1, 2, \ldots, N \end{aligned} \tag{4}$$

where $\boldsymbol{u} \in \mathbb{R}^3$ is the virtual command torque from the high-level controller. Matrices $\boldsymbol{H} \in \mathbb{R}^{3\times 3}$ and $\boldsymbol{M} \in \mathbb{R}^{3\times 3}$ are positive-definite weighting matrices.

The first term of $J_e$ is related to the CA error $\boldsymbol{D}\boldsymbol{\tau} - \boldsymbol{u}$, and the second term relates to reducing energy consumption. Different from the static CA problem in [7,8], the CA error $\boldsymbol{D}\boldsymbol{\tau} - \boldsymbol{u}$ is involved in the objective function, because we may not find appropriate values of $\boldsymbol{\tau}$ at any time to ensure $\boldsymbol{D}\boldsymbol{\tau} - \boldsymbol{u} = 0$ if the output saturation of the actuator is considered. In view of this, the proposed static CA problem in Eq. (4) minimizes the CA error $\boldsymbol{D}\boldsymbol{\tau} - \boldsymbol{u}$ instead of forcing CA error to be zero (e.g., $\boldsymbol{D}\boldsymbol{\tau} - \boldsymbol{u} = 0$).

### C. Necessary Lemmas and Definitions

The following lemmas and definitions will be used in deriving the main conclusions of this work.

*Lemma 1 ([13] Lemma 1):* Suppose that $V(x): \mathbb{R}^n \to \mathbb{R}_+ \cup \{0\}$ is a continuous positive definite and radially unbounded function such that

$$D^+V(x(t)) \le -(\alpha V^p(x(t)) + \beta V^q(x(t)))^k \tag{5}$$

where $D^+V(x(t))$ denotes the upper right-hand derivative of $V(x(t))$, and $\alpha$, $\beta$, $p$, $q$, and $k$ are positive constants satisfying $pk < 1$ and $qk > 1$. Then, the origin of the nonlinear autonomous system $\dot{x}(t) = f(x(t))$ with $x(0) = x_0$ is fixed-time stable and the settling time can be estimated as

$$T \le T_{\max} = \frac{1}{\alpha^k(1 - pk)} + \frac{1}{\beta^k(qk - 1)} \tag{6}$$

*Definition 1 ([14] Definition 1):* The appointed-time prescribed performance function (ATPPF) is any continuous performance function $\rho(t)$ satisfying the following properties:

1) $\rho(t) > 0$,

2) $\dot{\rho}(t) \le 0$,

3) $\lim_{t\to T_f}\rho(t) = \rho_{T_f} > 0$ and for any $t \ge T_f$, $\rho(t) = \rho_{T_f}$, where $T_f$ is the prescribed appointed time and $\rho_{T_f}$ is the small steady-state constant error upper bound.

## III. Problem Statement

The objective of this paper is to design an attitude control scheme for overactuated spacecraft to achieve fast and high-precision attitude tracking despite the actuator output saturation. As shown in Fig. 1, there are two parts of the proposed attitude control scheme for overactuated spacecraft: 1) the high-level controller that accounts for attitude stabilization; 2) the low-level prescribed performance ACA for realizing the commanded control torque from high-level controller. In the design process, the high-level and low-level structures can be designed independently [1].

The high-level controller for the spacecraft attitude redirection can be designed by various nonlinear control methods, such as sliding mode control [15], adaptive control [16], backstepping control [17], fuzzy adaptive control [18], hybrid control [19], inverse optimal control [20], and nonlinear model predictive control [21]. Because this paper mainly focuses on low-level CA, a simple saturated PD controller is used as high-level controller to achieve asymptotic spacecraft attitude stabilization and provide the virtual command torque $\boldsymbol{u}$. In light of the kinematics function (1) and the attitude dynamics (3) of rigid spacecraft, a high-level attitude controller can be designed as

$$\boldsymbol{u} = -k_p\boldsymbol{q}_e - k_d\mathrm{Tanh}\left(\frac{\boldsymbol{\omega}}{r^2}\right) \tag{7}$$

where $k_p$ and $k_d$ are positive constants, $\mathrm{Tanh}(\omega/r^2) = [\tanh(\omega_1/r^2), \tanh(\omega_2/r^2), \tanh(\omega_3/r^2)]^T$, and $r^2$ is a nonzero scalar sharpness function satisfying $0 < r^2_{\min} \le r^2 \in \ell_\infty$ and $\dot{r} \in \ell_\infty$. Then, the zero-disturbance closed-loop system is asymptotically stable, i.e., $\lim_{t\to\infty}\boldsymbol{\omega}(t) = 0$ and $\lim_{t\to\infty}\boldsymbol{q}_e(t) = 0$. The stability can be guaranteed by following the same analysis in ([22] Lemma 1) with a Lyapunov-like function given as $V_C = k_p[\boldsymbol{q}_e^T\boldsymbol{q}_e + (1 - q_{e0})^2] + (1/2)\boldsymbol{\omega}^T\boldsymbol{J}\boldsymbol{\omega}$.

*Remark 1:* Since, $\|\boldsymbol{q}_e\| \in [0, 1]$ and $\mathrm{Tanh}(\boldsymbol{\omega}/r^2) \in [0, 1]$,

$$\begin{aligned} \|\boldsymbol{u}\| &= \left\| -k_p\boldsymbol{q}_e - k_d\mathrm{Tanh}\left(\frac{\boldsymbol{\omega}}{r^2}\right)\right\| \le k_p\|\boldsymbol{q}_e\| + k_d\left\|\mathrm{Tanh}\left(\frac{\boldsymbol{\omega}}{r^2}\right)\right\| \\ &\le k_p + k_d \end{aligned} \tag{8}$$

can be obtained. Therefore, the commanded torque range of the high-level controller can be controlled by adjusting the values of the proportional coefficient $k_p$ and the differential coefficient $k_d$. However, too large $k_p$ and $k_d$ values can make the command torque of the high-level controller too large, which may lead to the failure of the CA algorithm. Therefore, it is necessary to select the values of $k_p$ and $k_d$ reasonably.

Then, based on the high-level controller (7), the following problem is solved:

*Problem 1 (low-level ATPP-FixTACA):* Under the output limitation of actuators, design an appointed-time prescribed performance-

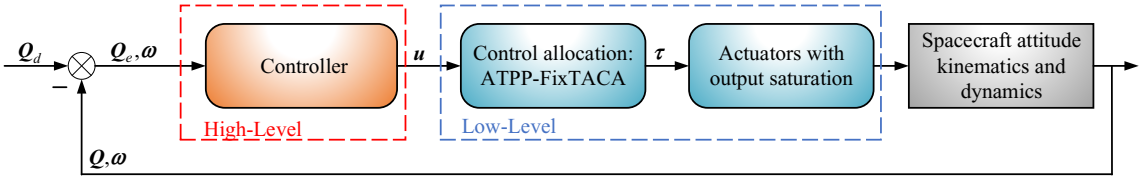


**Fig. 1 Structure diagram of the overall attitude control system.**

based fixed-time adaptive control allocation (ATPP-FixTACA) to dynamically assign the virtual command torque provided by the high-level controller to each actuator.

## IV. Prescribed Performance Adaptive Control Allocation

In this section, an ATPP-FixTACA approach is proposed, which can distribute the desired/virtual control torque to each actuator dynamically. Firstly, the constrained ACA problem is transformed into the barrier-function-based unconstrained ACA problem. Then the appointed-time prescribed performance (ATPP) function is established for the ACA problem to predefine the transient and steady-state ACA performance. Finally, we show that the proposed ACA approach can guarantee the fixed-time convergence of the ACA error.

### A. Transformed CA Problem

To transform the constrained optimization CA (4) into an unconstrained one, the barrier function is used in [23 (Chap. 19.1) and [9]. The barrier-function-based unconstrained ACA problem corresponding to Eq. (4) is defined as

$$L(\boldsymbol{\tau},\boldsymbol{u}) = \frac{1}{2}(\boldsymbol{D\tau}-\boldsymbol{u})^T\boldsymbol{H}(\boldsymbol{D\tau}-\boldsymbol{u}) + \frac{1}{2}\boldsymbol{\tau}^T\boldsymbol{M\tau} - P\sum_{l=1}^{2}\sum_{i=1}^{N}\log(C_{l,i}(\tau_i)) \tag{9}$$

where $P$ is a positive weight constant, and the functions $C_{1,i} = \tau_i - \tau_{i,\min}$ and $C_{2,i} = \tau_{i,\max} - \tau_i$ with $i \in \{1, \ldots, N\}$. The minimization of the barrier term $-P\sum_{l=1}^{2}\sum_{i=1}^{N}\log(C_{l,i}(\tau_i))$ in Eq. (9) prevents the components of $C_{1,i}$ and $C_{2,i}$ from becoming too close to zero (recall that $-\log(x) \to \infty$, as $x \to 0$). This operation ensures that the CA meets the actuator output saturation constraint. The approximation accuracy improves as the positive parameter $P$ decreases. In the extreme case when $P = 0$, the transformed program has no constraint on the output of the actuators.

*Assumption 1:* The initial output of the each actuator is assumed to satisfy inequality constraints $C_{1,i} > 0$ and $C_{2,i} > 0$.

Therefore, the barrier-function-based unconstrained CA problem is formulated as

$$\min_{\boldsymbol{\tau}} L(\boldsymbol{\tau},\boldsymbol{u}) \tag{10}$$

The first-order optimal set of Eq. (10) can be defined as

$$\mathcal{Z} = \left\{\boldsymbol{\tau}\,\middle|\,\frac{\partial L}{\partial \boldsymbol{\tau}} = 0\right\} \tag{11}$$

where

$$\frac{\partial L}{\partial \boldsymbol{\tau}} = \boldsymbol{D}^T\boldsymbol{H}^T(\boldsymbol{D\tau}-\boldsymbol{u}) + \boldsymbol{M}^T\boldsymbol{\tau} - P(\boldsymbol{\tau}_{r,\min} - \boldsymbol{\tau}_{r,\max}) \tag{12}$$

with

$$\boldsymbol{\tau}_{r,\min} \triangleq \left[\frac{1}{\tau_1-\tau_{1,\min}},\ldots,\frac{1}{\tau_N-\tau_{N,\min}}\right]^T \in \mathbb{R}^N$$

and

$$\boldsymbol{\tau}_{r,\max} \triangleq \left[\frac{1}{\tau_{1,\max}-\tau_1},\ldots,\frac{1}{\tau_{N,\max}-\tau_N}\right]^T \in \mathbb{R}^N$$

*Lemma 2:* The local minimum of the barrier-function-based unconstrained CA problem (10) is achieved if and only if the optimal set $\mathcal{Z}$ holds.

*Proof:* Necessity: The first necessary optimal condition is satisfied if the set $\mathcal{Z}$ is reached [7,23]. Then, the CA problem in Eq. (10) achieves its local minimum.

Sufficiency: According to the second-order sufficient condition, the local minima is achieved if $(\partial L/\partial \boldsymbol{\tau}) = 0$ and $(\partial^2 L/\partial \boldsymbol{\tau}^2) > 0$. From Eq. (12), we have

$$\frac{\partial^2 L}{\partial \boldsymbol{\tau}^2} = \boldsymbol{D}^T\boldsymbol{H}^T\boldsymbol{D} + \boldsymbol{M}^T + P\mathrm{diag}\{\boldsymbol{\tau}_{r^2,\min} + \boldsymbol{\tau}_{r^2,\max}\} \tag{13}$$

where

$$\boldsymbol{\tau}_{r^2,\min} \triangleq \left[\frac{1}{(\tau_1-\tau_{1,\min})^2},\ldots,\frac{1}{(\tau_N-\tau_{N,\min})^2}\right]^T \in \mathbb{R}^N$$

and

$$\boldsymbol{\tau}_{r^2,\max} \triangleq \left[\frac{1}{(\tau_{1,\max}-\tau_1)^2},\ldots,\frac{1}{(\tau_{N,\max}-\tau_N)^2}\right]^T \in \mathbb{R}^N$$

Since the third term in Eq. (13) is a positive definite diagonal matrix, $(\partial^2 L/\partial \tau^2) > 0$ can be obtained. Therefore, the sufficiency is guaranteed. □

*Remark 2:* The CA error $\boldsymbol{D\tau} - \boldsymbol{u}$ is related to $\partial L/\partial \boldsymbol{\tau}$ in Eq. (12). In view of the expression of $\partial L/\partial \boldsymbol{\tau}$, if a weight matrix $H \gg M$ and a small weight P are selected, $\partial L/\partial \boldsymbol{\tau}$ approximates $\boldsymbol{D}^T\boldsymbol{H}^T(\boldsymbol{D\tau}-\boldsymbol{u})$. Thus, when $\partial L/\partial \boldsymbol{\tau}$ approaches 0, $\boldsymbol{D\tau}-\boldsymbol{u}$ also approaches 0.

*Remark 3:* It is worth noting that we do not have to choose that the commanded control torque defined by the bound $k_p + k_d$ is equal to the actual control torque $\max_{\tau_{i,\min}\le\tau_i\le\tau_{i,\max}}\|\boldsymbol{D\tau}\|$ determined by the actuator saturation constraints. In this work, the maximum value of the commanded control torque is greater than the maximum value of the actual control torque of the actuators. For example, in the simulation, we select $k_p = 1$, $k_d = 0.6$, and $|\tau_i| \le 0.25$ N · m, which lead to

$$\max_{\boldsymbol{u}}\|\boldsymbol{u}\| = k_p + k_d = 1.6 \text{ N}\cdot\text{m},$$
$$\max_{\tau_{i,\min}\le\tau_i\le\tau_{i,\max}}\|\boldsymbol{D\tau}\| = 0.5774 \text{ N}\cdot\text{m}$$

It can be seen that the commanded control torque defined by the high-level controller exceeds the actual torque of the actuators.

### B. Appointed-Time Prescribed Performance Function

Before giving the details of the proposed ACA design, we construct an appointed-time prescribed performance (ATPP) function to predefine the transient and steady-state performance of the ACA. Inspired by [14] and Lemma 1, we can choose the ATPP function as follows:

$$\rho(t) = \begin{cases} a_3t^3 + a_2t^2 + a_1t + a_0, & \text{if } 0 \le t < T_f \\ \rho_{T_f}, & \text{if } t \ge T_f, \end{cases} \tag{14}$$

where the prescribed performance requirements on the initial value, steady-state error, and appointed convergence time are denoted by $\rho(0)$, $\rho_{T_f}$, and $T_f$, respectively. The variables $a_0$, $a_1$, $a_2$, and $a_3$ are coefficients to be designed such that the following constraints are satisfied:

$$\rho(0) = \rho_0, \dot{\rho}(0) = 0, \rho(t|t \ge T_f) = \rho_{T_f}, \dot{\rho}(t|t \ge T_f) = 0, \rho_0 > \rho_{T_f} > 0 \tag{15}$$

where $\dot{\rho}(0) = 0$ ensures that predefined error at the initial stage does not change too quickly. The condition $\dot{\rho}(t|t \ge T_f) = 0$ ensures that the predefined error $\rho(t|t \ge T_f) = \rho_{T_f}$ does not ultimately change.

Given the corresponding values of $\rho(0)$, $\rho_{T_f}$, and $T_f$, the ATPP function can be obtained by combining Eqs. (14) and (15).

*Remark 4:* In [14], an ATPP function is designed as

$$\rho(t) = \begin{cases} \left(\rho_0 - \dfrac{t}{T_f}\right) e^{\left(1 - \dfrac{T_f}{T_f - t}\right)} + \rho_{T_f}, & \text{if } 0 \le t < T_f \\ \rho_{T_f}, & \text{if } t \ge T_f \end{cases} \tag{16}$$

where $\rho_0$ is a specified parameter satisfying $\rho_0 \ge 1$ [14], which means that the initial value of the ATPP function has to be greater than 1. Otherwise, as $\rho_0 - t/T_f \le 0$, $\rho(t) < 0$ is obtained. In contrast, the proposed ATPP function in Eq. (14) avoids this constraint on $\rho_0$, and only needs to satisfy $\rho_0 = a_0 > 0$. Compared with the ATPP function (16) of [14], the proposed one can be applied to systems with a large allowable initial error.

Then, let the barrier-function-based CA error be $\boldsymbol{e} = (\partial L/\partial \boldsymbol{\tau}) \in \mathbb{R}^N$. The prescribed performance requirements on the barrier-function-based CA error $\boldsymbol{e}$ can be constructed by the following inequality:

$$-\boldsymbol{l} \odot \boldsymbol{\rho}(t) < \boldsymbol{e}(t) < \boldsymbol{h} \odot \boldsymbol{\rho}(t), \quad \forall\, t \ge 0 \tag{17}$$

where the symbol $\odot$ denotes the Hadamard product, $\boldsymbol{\rho}(t) = [\rho_1(t), \cdots, \rho_N(t)]^T \in \mathbb{R}^N$ is the ATPP function of $\boldsymbol{e}(t)$, and $\boldsymbol{l} = [l_1, \cdots, l_N]^T \in \mathbb{R}^N$ and $\boldsymbol{h} = [h_k, \cdots, h_N]^T \in \mathbb{R}^N$ are two positive weighting vectors of $\boldsymbol{\rho}(t)$ satisfying $\mathbf{0}_N < \boldsymbol{l} \le \mathbf{1}_N$ and $\mathbf{0}_N < \boldsymbol{h} \le \mathbf{1}_N$. The transient and steady-state performance of $\boldsymbol{e}(t)$ can be set by selecting different parameters in $\boldsymbol{\rho}(t)$, $\boldsymbol{l}$ and $\boldsymbol{h}$. Next, a smooth invertible function is introduced as $\boldsymbol{S}(\boldsymbol{z}) = [S_1(z_1), \cdots, S_N(z_N)]^T$ with

$$S_i(z_i) = \frac{h_i e^{z_i} - l_i e^{-z_i}}{e^{z_i} + e^{-z_i}}, \qquad i = 1, 2, \cdots, N \tag{18}$$

Utilizing $\boldsymbol{S}(\boldsymbol{z})$, we can transform the performance constraints in Eq. (17) into the following form:

$$\boldsymbol{e}(t) = \boldsymbol{\rho}(t) \odot \boldsymbol{S}(\boldsymbol{z}) \tag{19}$$

where $\boldsymbol{z} = [z_1, \cdots z_N]^T \in \mathbb{R}^N$ is the conversion error. Since $\boldsymbol{S}(\boldsymbol{z})$ is the strictly monotone increasing function and $\boldsymbol{\rho}_0 > \boldsymbol{\rho}_{T_f} > 0$, we can get the corresponding inverse transformation as

$$z_i = S_i^{-1}(\beta_i(t)) = \frac{1}{2} \ell_n \left(\frac{l_i + \beta_i(t)}{h_i - \beta_i(t)}\right), \qquad i = 1, 2, \cdots N \tag{20}$$

where $\beta_i(t) = e_i(t)/\rho_i(t)$. Then, assume that the barrier-function-based CA error $\boldsymbol{e}(0)$ satisfies (17), and the constraints (17) from the prescribed performance can be satisfied by converging the conversion errors into the following set:

$$\mathcal{Z}^* = \{\boldsymbol{z} | \boldsymbol{z} = 0\} \tag{21}$$

*Remark 5:* Since $\boldsymbol{l}$ and $\boldsymbol{h}$ are two weight vectors, the prescribed performance requirements on the barrier-function-based CA error $\boldsymbol{e}$ at the initial time are mainly determined by $\boldsymbol{\rho}(0)$. Therefore, a larger value of $\boldsymbol{\rho}(0)$ is selected to meet the inequality (17) at $t = 0$. However, too large $\boldsymbol{\rho}(0)$ will weaken the effect of the ATPP function. For example, consider one-dimensional vector; set $l = h = 1$, $T_f = 5$ s, and $\rho_{T_f} = 0.001$; and then take $\rho_0 = 0.3$, $\rho_0 = 0.6$, $\rho_0 = 1$, and $\rho_0 = 3$, respectively. The results are shown in Fig. 2. It is obvious that a larger $\rho_0$ has less ability to constrain the dynamic performance of the CA error $\boldsymbol{e}$. Therefore, choosing an appropriate $\boldsymbol{\rho}(0)$ is critical to the transient performance of the system.

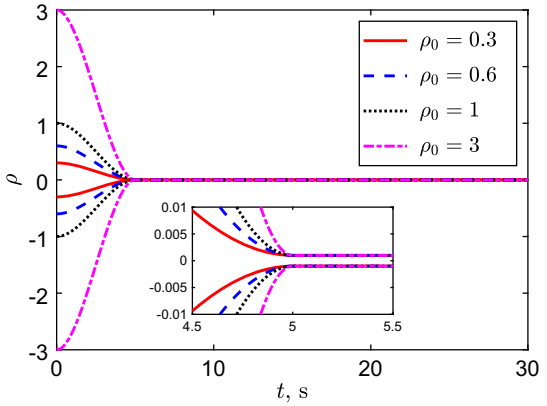


**Fig. 2 The ATPP functions $\rho$ with different initial values.**

### C. Fixed-Time Adaptive Control Allocation

Motivated by [6], to dynamically converge the barrier-function-based CA error in fixed time while satisfying the transient and steady-state performance defined by ATPP function, an updating law of $\boldsymbol{\tau}$ that drives to reach the set $\mathcal{Z}^*$ is proposed as

$$\dot{\boldsymbol{\tau}} = -k_1 \boldsymbol{G}^T \boldsymbol{R}^{-1} \mathrm{sig}_1(z) - k_2 \boldsymbol{G}^T \boldsymbol{R}^{-1} \mathrm{sig}_2(z) + \boldsymbol{R}^{-1} \boldsymbol{\phi} \tag{22}$$

where $\boldsymbol{G} = (\partial^2 L/\partial \boldsymbol{\tau}^2)$,

$$\boldsymbol{R} = \mathrm{diag}\left(\frac{\partial S^{-1}(\beta_i(t))}{\partial \beta_i(t)} \cdot \frac{1}{\rho_i(t)}\right)$$

with $i = 1, \cdots N$, $\mathrm{sig}_1(\boldsymbol{x}) = [|x_1|^\gamma \mathrm{sign}(x_1), \cdots, |x_m|^\gamma \mathrm{sign}(x_m)]^T$, $\mathrm{sig}_2(\boldsymbol{x}) = [|x_1|^{\gamma+1} \mathrm{sign}(x_1), \cdots, |x_m|^{\gamma+1} \mathrm{sign}(x_m)]^T$ with $0 < \gamma < 1$ and $m$ representing the number of elements in the column vector $\boldsymbol{x}$, and $\boldsymbol{\phi} \in \mathbb{R}^N$ can be obtained by solving the least-square problem with a scalar time-varying algebraic equation given by [9]

$$\boldsymbol{z}^T \boldsymbol{G}^T \boldsymbol{\phi} + \boldsymbol{z}^T \boldsymbol{R} \left(-\boldsymbol{\beta} \odot \dot{\boldsymbol{\rho}} + \frac{\partial^2 L}{\partial \boldsymbol{u} \partial \boldsymbol{\tau}} \dot{\boldsymbol{u}}\right) = 0 \tag{23}$$

Now, we are ready to present the ATPP-FixTACA result for the barrier-function-based unconstrained CA problem (10).

*Theorem 1:* The updating law in Eq. (22) can result in $\boldsymbol{z}^T \to \mathcal{Z}^*$ in fixed time; thus, the barrier-function-based unconstrained CA problem (10) is solved.

*Proof:* Choose a Lyapunov-like function as follows:

$$V_A(\boldsymbol{u}, \boldsymbol{z}) = \frac{1}{2} \boldsymbol{z}^T \boldsymbol{z} \tag{24}$$

It is obvious from Eq. (12) that $\partial^2 L_2/\partial t \partial \boldsymbol{\tau} = 0$. Thus, time derivative of $V_A(\boldsymbol{u}, \boldsymbol{z})$ is

$$\dot{V}_A = \boldsymbol{z}^T \boldsymbol{R} \left(\boldsymbol{G} \dot{\boldsymbol{\tau}} + \left(-\boldsymbol{\beta} \odot \dot{\boldsymbol{\rho}} + \frac{\partial^2 L}{\partial \boldsymbol{u} \partial \boldsymbol{\tau}} \dot{\boldsymbol{u}}\right)\right) \tag{25}$$

Substituting Eqs. (22) and (23) into the foregoing equation yields

$$\dot{V}_A = -k_1 \boldsymbol{z}^T \boldsymbol{R} \boldsymbol{G} \boldsymbol{G}^T \boldsymbol{R}^{-1} \mathrm{sig}_1(z) - k_2 \boldsymbol{z}^T \boldsymbol{R} \boldsymbol{G} \boldsymbol{G}^T \boldsymbol{R}^{-1} \mathrm{sig}_2(z) \tag{26}$$

According to the definition of $\boldsymbol{G}$ in Eq. (13), it is obvious that $\boldsymbol{G}$ is nonsingular, and $\boldsymbol{G}^T \boldsymbol{G}$ is a positive-definite matrix. Furthermore, we have the eigenvalues of $\boldsymbol{G}^T \boldsymbol{G}$ are bounded; i.e., $0 < \lambda_{\min} \le \lambda(\boldsymbol{G}^T \boldsymbol{G}) \le \lambda_{\max}$ is satisfied, where $\lambda_{\min}$ and $\lambda_{\max}$ represent the minimum eigenvalue and the maximum eigenvalue of matrix $\boldsymbol{G}^T \boldsymbol{G}$, respectively. Meanwhile, due to the fact $-\boldsymbol{R} \boldsymbol{G} \boldsymbol{G}^T \boldsymbol{R}^{-1} \le -\lambda_{\min} \boldsymbol{I}_N$, it follows from Eq. (26) that

$$\begin{aligned}\dot{V}_A &\le \lambda_{\min}(-k_1\|z\|^{1+\gamma} - k_2\|z\|^{2+\gamma}) \\ &\le -2^{\frac{1+\gamma}{2}}\lambda_{\min}k_1 V_A^{\frac{1+\gamma}{2}} - 2^{\frac{2+\gamma}{2}}\lambda_{\min}k_2 V_A^{\frac{2+\gamma}{2}}\end{aligned} \tag{27}$$

where $0 < [(1+\gamma)/2] < 1$ and $1 < [(2+\gamma)/2] < 2$. Therefore, according to the fixed-time convergence theory given in Lemma 1, the optimal set $\mathcal{Z}^*$ is reached in the fixed time given by

$$T_{\text{reach}} \le \frac{1}{2^{\frac{1+\gamma}{2}}\lambda_{\min}k_1\left(1-\frac{1+\gamma}{2}\right)} + \frac{1}{2^{\frac{2+\gamma}{2}}\lambda_{\min}k_2\left(\frac{2+\gamma}{2}-1\right)} \tag{28}$$

This completes the proof. □

Moreover, according to Eq. (20), if $\mathcal{Z}^*$ is achieved in fixed time $T_{\text{reach}}$, then the following condition

$$\boldsymbol{e} = \frac{\partial L}{\partial \boldsymbol{\tau}} = \frac{\boldsymbol{h}-\boldsymbol{l}}{2} \odot \boldsymbol{\rho}(t) \tag{29}$$

is also guaranteed in fixed time $T_{\text{reach}}$. If we choose $\boldsymbol{h} = \boldsymbol{l}$ then $\boldsymbol{e} = \boldsymbol{0}$, which means that the first-order optimal set $\mathcal{Z}$ of the barrier-function-based unconstrained CA problem in Eq. (10) can be reached in fixed time $T_{\text{reach}}$; i.e., the proposed ATPP-FixTACA approach not only achieves fixed-time convergence of the barrier-function-based unconstrained CA error, but also guarantees the transient and steady-state performance requirements defined by the ATPP function.

*Remark 6:* The fixed time $T_{\text{reach}}$ at which the optimal set $\mathcal{Z}^*$ is reached is only related to the parameters $\gamma$, $k_1$, $k_2$, $\boldsymbol{D}$, $\boldsymbol{H}$, $\boldsymbol{M}$, and P of the proposed ATPP-FixTACA. Once the parameters are selected, the fixed time $T_{\text{reach}}$ can be calculated by Eq. (28).

*Remark 7:* According to Eq. (29), the barrier-function-based unconstrained CA error $\boldsymbol{e}$ is ultimately determined by $\boldsymbol{h}$, $\boldsymbol{l}$, and $\boldsymbol{\rho}$. The barrier-function-based unconstrained CA error $\boldsymbol{e}$ reaching the first-order optimality set $\mathcal{Z}$ is determined by $T_f$, and the gains $\gamma$, $k_1$, and $k_2$ determine the convergence speed. Specifically, smaller $\gamma$ and larger $k_1$ and $k_2$ can lead to faster $\boldsymbol{e}$ convergence rate, but unnecessary oscillation may occur.

*Remark 8:* In this work, the analytical solution of $\dot{\boldsymbol{u}}$ in Eq. (23) can be obtained through the high-level controller (7). For complex controllers, there are also many methods to obtain $\dot{\boldsymbol{u}}$ approximately, such as the low-pass filter [24] and the first-order Levant differentiator [25,26].

*Remark 9:* If the prescribed performance is not considered, the fixed-time adaptive control allocation (FixT-ACA) law can be derived as follows:

$$\dot{\boldsymbol{\tau}} = -k_1\boldsymbol{G}\text{sig}_1\left(\frac{\partial L}{\partial \boldsymbol{\tau}}\right) - k_2\boldsymbol{G}\text{sig}_2\left(\frac{\partial L}{\partial \boldsymbol{\tau}}\right) + \boldsymbol{\phi}^* \tag{30}$$

where $\boldsymbol{\phi}^* \in \mathbb{R}^N$ is obtained by solving the following scalar time-varying algebraic equation:

$$\left(\frac{\partial L}{\partial \boldsymbol{\tau}}\right)^T \boldsymbol{G}\boldsymbol{\phi}^* + \left(\frac{\partial L}{\partial \boldsymbol{\tau}}\right)^T \frac{\partial^2 L}{\partial \boldsymbol{u}\partial \boldsymbol{\tau}}\dot{\boldsymbol{u}} = 0 \tag{31}$$

In addition, the fixed-time stability can be guaranteed by following the same analysis in [9] with a Lyapunov-like function given as

$$\bar{V}_A(\boldsymbol{u},\boldsymbol{\tau}) = \frac{1}{2}\left(\frac{\partial L}{\partial \boldsymbol{\tau}}\right)^T \frac{\partial L}{\partial \boldsymbol{\tau}} \tag{32}$$

## V. Overall Closed-Loop Stability

The stability of the overall closed-loop system including the high-level controller in Eq. (7) and low-level ATPP-FixTACA in Eq. (22) is summarized in the following theorem.

*Theorem 2:* Consider the attitude control systems expressed in Eqs. (1) and (3) with the high-level controller in Eq. (7) and the low-level ATPP-FixTACA in Eq. (22). If the condition

$$k_d > \frac{1}{2} \tag{33}$$

is satisfied, then the state variables $(\boldsymbol{\omega}^T, \boldsymbol{z}^T)^T$ are uniformly ultimately bounded in the sense of converging to small invariant sets containing the origin, i.e., $\lim_{t\to\infty}\|\boldsymbol{\omega}\| \in \Omega_{\boldsymbol{\omega}}$ and $\lim_{t\to\infty}\|\boldsymbol{z}\| \in \Omega_z$, where

$$\Omega_{\boldsymbol{\omega}} = \left\{\boldsymbol{\omega} | \boldsymbol{\omega}^T\text{sign}(\boldsymbol{\omega}) \le \sqrt{\frac{\eta}{k_d - \frac{1}{2}}}\right\}$$

$\Omega_z = \{\boldsymbol{z} | \|\boldsymbol{z}\| \le g(\eta, k_1, k_2)\}$ with $\eta \triangleq (1/2)\|\boldsymbol{D}\boldsymbol{\tau} - \boldsymbol{u}\|^2 + |\varepsilon|$ and

$$g(\eta, k_1, k_2) \triangleq \max\left(\sqrt{\frac{\eta}{k_1\lambda_{\min}}}, \sqrt{\frac{\eta}{k_2\lambda_{\min}}}\right)$$

where $\varepsilon = \boldsymbol{\omega}^T\text{sign}(\boldsymbol{\omega}) - \boldsymbol{\omega}^T\text{Tanh}(\boldsymbol{\omega}/r^2)$.

*Proof:* Selecting a Lyapunov-like function as

$$V = V_C + V_A \tag{34}$$

In view of Eq. (27), the time derivative of $V$ is

$$\begin{aligned}\dot{V} &= (k_p\boldsymbol{q}_e^T\boldsymbol{\omega} + \boldsymbol{\omega}^T(\boldsymbol{u} + \boldsymbol{D}\boldsymbol{\tau} - \boldsymbol{u})) - k_1\lambda_{\min}\|\boldsymbol{z}\|^{1+\gamma} - k_2\lambda_{\min}\|\boldsymbol{z}\|^{2+\gamma} \\ &= -k_d\boldsymbol{\omega}^T\text{Tanh}\left(\frac{\boldsymbol{\omega}}{r^2}\right) + \boldsymbol{\omega}^T(\boldsymbol{D}\boldsymbol{\tau} - \boldsymbol{u}) - k_1\lambda_{\min}\|\boldsymbol{z}\|^{1+\gamma} \\ &\quad - k_2\lambda_{\min}\|\boldsymbol{z}\|^{2+\gamma} \\ &\le -k_d\boldsymbol{\omega}^T\text{sign}(\boldsymbol{\omega}) + |\varepsilon| + \frac{1}{2}\|\boldsymbol{\omega}\|^2 + \frac{1}{2}\|\boldsymbol{D}\boldsymbol{\tau} - \boldsymbol{u}\|^2 \\ &\quad - k_1\lambda_{\min}\|\boldsymbol{z}\|^{1+\gamma} - k_2\lambda_{\min}\|\boldsymbol{z}\|^{2+\gamma} \\ &\le -\left(k_d - \frac{1}{2}\right)\boldsymbol{\omega}^T\text{sign}(\boldsymbol{\omega}) - k_1\lambda_{\min}\|\boldsymbol{z}\|^{1+\gamma} - k_2\lambda_{\min}\|\boldsymbol{z}\|^{2+\gamma} + \eta\end{aligned} \tag{35}$$

where the fact $\|\boldsymbol{\omega}\| \le \boldsymbol{\omega}^T\text{sign}(\boldsymbol{\omega})$ is used. Since $\varepsilon$, $\boldsymbol{D}\boldsymbol{\tau}$, and $\boldsymbol{u}$ are bounded, $\eta$ is bounded.

Clearly, choosing $k_d$ such that the condition in Eq. (33) is satisfied, and according to Eq. (35), we can obtain that $\dot{V} < 0$ if

$$\boldsymbol{\omega}^T\text{sign}(\boldsymbol{\omega}) > \sqrt{\frac{\eta}{k_d - \frac{1}{2}}}$$

or $\|\boldsymbol{z}\| > g(\eta, k_1, k_2)$, where

$$g(\eta, k_1, k_2) \triangleq \max\left(\sqrt{\frac{\eta}{k_1\lambda_{\min}}}, \sqrt{\frac{\eta}{k_2\lambda_{\min}}}\right)$$

As a result, the spacecraft state vector $\boldsymbol{\omega}$ and conversion error $\boldsymbol{z}$ are uniformly ultimately bounded, and converge to invariant sets containing the origin as $t \to \infty$. □

## VI. Simulation Results

To demonstrate the effectiveness of the proposed attitude controller and the ATPP-FixTACA, numerical simulation for the overactuated spacecraft with actuator output saturation is carried out. For the spacecraft, the rigid part of the inertia matrix is given as

$$\boldsymbol{J} = \begin{bmatrix} 20 & 1.2 & 0.9 \\ 1.2 & 17 & 1.4 \\ 0.9 & 1.4 & 15 \end{bmatrix} \text{kg}\cdot\text{m}^2$$

Moreover, four reaction wheels are used as actuators, whose distribution matrix

$$\boldsymbol{D} = \frac{1}{\sqrt{3}}\begin{bmatrix} -1 & -1 & 1 & 1 \\ 1 & -1 & -1 & 1 \\ 1 & 1 & 1 & 1 \end{bmatrix}$$

is the same as [9]. Each reaction wheel has to satisfy the saturation constraint $|\tau_n| \leq 0.25$ N · m for $n \in \{1, \ldots 4\}$.

The numerical simulation results are given based on the following two scenarios:

*Scenario 1:* The initial attitude is $\boldsymbol{Q}(0) = [0.1092, 0, -0.4624, 0.8799]^T$ and the desired attitude is given as $\boldsymbol{Q}_d = [0.5624, -0.5689, 0, 0.6]^T$. The initial angular velocity is assumed to be $\boldsymbol{\omega}(0) = [0, 0, 0]^T$ deg /s.

*Scenario 2:* The initial attitude is $\boldsymbol{Q}(0) = [0.5624, -0.5689, 0, 0.6]^T$ and the desired attitude is given as $\boldsymbol{Q}_d = [1, 0, 0, 0]^T$. The initial angular velocity is assumed to be $\boldsymbol{\omega}(0) = [-2, 3, -2]^T$ deg /s.

### A. Overall Attitude Control Simulation Results

In this subsection, the overall performance of the proposed high-level controller in Eq. (7), combined with low-level ATPP-FixTACA in Eq. (22), is simulated. The parameters of the proposed attitude controller are set to $k_p = 1$ and $k_d = 0.6$. The parameters of the proposed ATPP-FixTACA scheme are set to $\boldsymbol{H} = 0.5\boldsymbol{I}_3$, $\boldsymbol{M} = 0.05\boldsymbol{I}_4$, $P = 0.002$, $\gamma = 0.6$, and $k_1 = k_2 = 10$. Meanwhile, the parameters of the ATPP are set to $\boldsymbol{\rho}_0 = [0.5, 0.5, 0.5]$, $T_f = 5$ s, $\boldsymbol{\rho}_{T_f} = [0.001, 0.001, 0.001]$, and $\boldsymbol{h} = \boldsymbol{l} = [1, 1, 1]$, and then, based on Eq. (14) and constraint (15), we can get $a_0 = \rho_0 = 0.5$, $a_1 = 0$, and the following two equations should also hold:

$$\begin{cases} a_3 T_f^3 + a_2 T_f^2 + a_0 = \rho_f \\ 3a_3 T_f^2 + 2a_2 T_f = 0 \end{cases}$$

Solving above equations, we can get $a_2 = -0.0599$ and $a_3 = 0.008$. Meanwhile, according to Eq. (28), the optimal set $\mathcal{Z}$ is reached in $T_{\text{reach}} \leq 32.5138$ s, which is greater than the appointed-time $T_f = 5$ s.

The numerical simulation results of scenario 1 and scenario 2 are shown in Figs. 3 and 4, respectively.

In scenario 1, the attitude error and angular velocity error are shown in Figs. 3a and 3b, from which we can see that the state errors converge to zero asymptotically with the steady-state errors $|\boldsymbol{q}_e| \leq 2 \times 10^{-4}$ and $|\boldsymbol{\omega}| \leq 2 \times 10^{-3}$ deg /s in 100 s. In scenario 2, the attitude error and angular velocity error are shown in Figs. 4a and 4b, from which we can see that the state errors converge to zero asymptotically with the steady-state errors $|\boldsymbol{q}_e| \leq 2 \times 10^{-4}$ and $|\boldsymbol{\omega}| \leq 2 \times 10^{-3}$ deg /s in 100 s.

The output torques of reaction wheels of the two scenario are shown in Figs. 3c and 4c, where it is observed that the reaction wheel saturation constraints are satisfied and the saturation limits of the actuators are not reached, i.e., $\tau_i < 0.25$ N · m for all $i \in \{1, \ldots, 4\}$.

Moreover, as shown in Figs. 3d and 4d, the first-order optimality set $\mathcal{Z}$ of the ACA problem can be reached in fixed time ($T_{\text{reach}} \leq 32.5138$ s) by applying the proposed ATPP-FixTACA method. In addition, the barrier-function-based unconstrained CA error $\boldsymbol{e}$ also meets the required performance defined by ATPP function (17) and converges to the set $\mathcal{Z}$ with steady-state error of level of $1 \times 10^{-10}$ in $t = 110$ s due to $\boldsymbol{h} = \boldsymbol{l} = [1, 1, 1]^T$, $\boldsymbol{\rho}_{T_f} = 10^{-3}$, which is consistent with the performance defined in Eq. (29). Therefore, the ATPP-FixTACA not only achieves fixed-time convergence of the barrier-function-based unconstrained CA error $\boldsymbol{e}$ but also guarantees appointed-time predefined ACA transient performance.

It is worth mentioning that not all initial states can be successfully simulated under these parameters of this work. When the initial CA error is large, the simulation may fail. On the one hand, larger $\boldsymbol{\rho}(0)$ and $T_f$ can be selected in the ATPP function. Then the appropriate $\boldsymbol{\rho}(0)$ and $T_f$ are determined through multiple numerical simulations to obtain better performance. On the other hand, larger values of $\boldsymbol{\rho}(0)$ and $T_f$ can also be directly selected, which can increase the robustness of the system to any initial state, but also increase the conservatism of CA.

In summary, the overall control scheme consisting of the high-level controller (7) and the low-level ATPP-FixTACA approach (22) can complete the attitude reorientation task for an overactuated spacecraft.

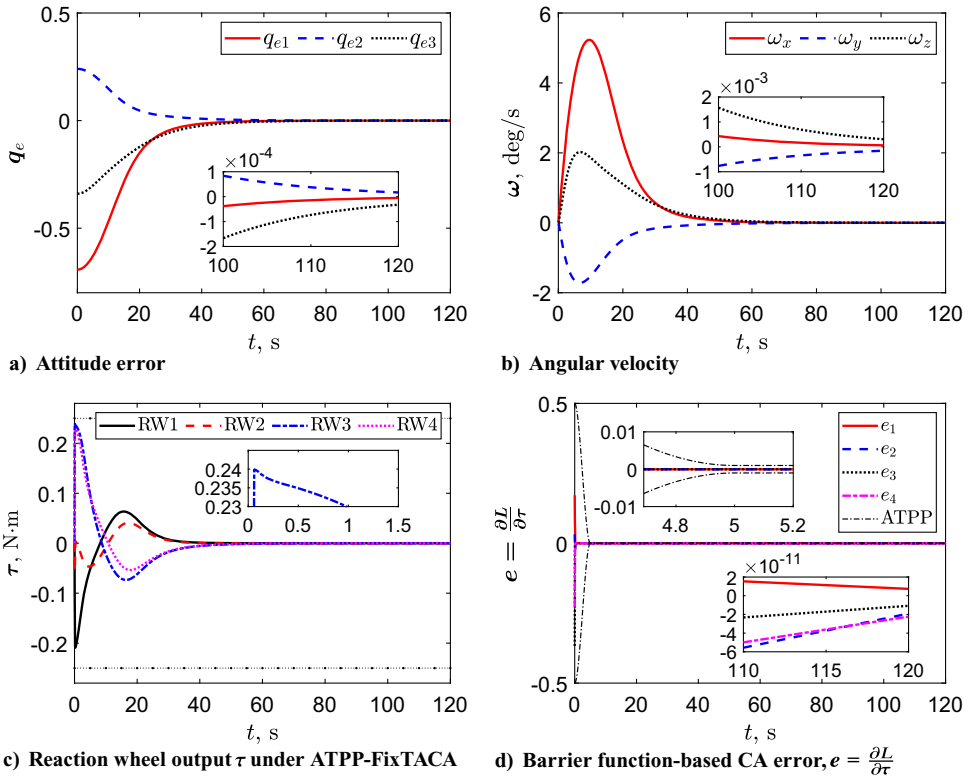


a) Attitude error

b) Angular velocity

c) Reaction wheel output $\tau$ under ATPP-FixTACA

d) Barrier function-based CA error, $\boldsymbol{e} = \frac{\partial L}{\partial \tau}$

**Fig. 3 Time history of the overall attitude control system under scenario 1.**

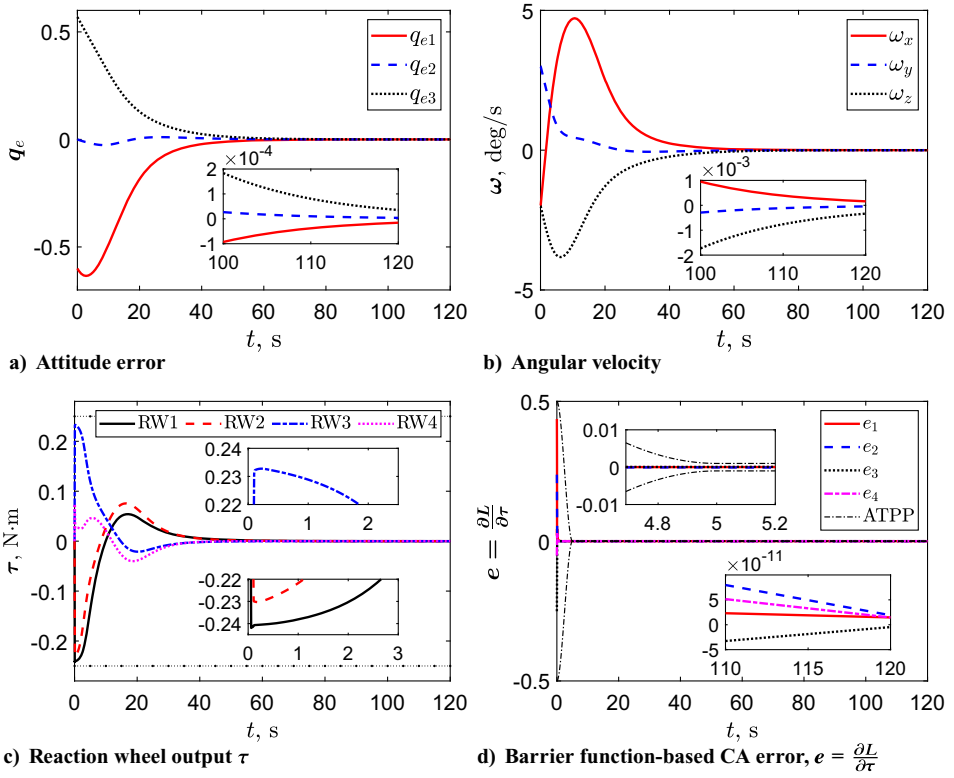


a) Attitude error b) Angular velocity

c) Reaction wheel output $\tau$ d) Barrier function-based CA error, $\boldsymbol{e} = \frac{\partial L}{\partial \tau}$

**Fig. 4 Time history of the overall attitude control system under scenario 2.**

### B. Low-Level ACA Comparison

In this subsection, the efficiency of the proposed ATPP-FixTACA approach in Eq. (22) is verified. To show the advantages of the proposed approach, the other two existing CA methods, i.e., the static pseudo-inverse-based CA (PICA) in [1], where $\boldsymbol{\tau} = \boldsymbol{D}^T(^T)^{-1}\boldsymbol{u}$, and the ACA in [8] are also simulated for comparison. The numerical simulation results are given based on scenario 1 as in the above subsection. Because the static PICA and ACA approaches do not consider the actuator saturation constraint, the saturation function is used to limit the actual output of the actuators of the two CA approaches. To have a fair comparison, we utilize the controller in Eq. (7) as a high-level attitude controller for all three CA approaches. The parameters of the ACA approaches are given as $\Gamma = W = 10$ and $\boldsymbol{M}_v = 0.05\boldsymbol{I}_4$.

As shown in Figs. 5a and 5b, compared with the ACA approach, the attitude error $\|\boldsymbol{q}_e\|$ of the proposed ATPP-FixTACA approach is smaller than those of the ACA approach and does not bring the problem of excessive angular velocity. This is because the ATPP function is used to improve the transient performance, and the fixed time convergence method is used to improve the convergence rate of allocation error in the proposed ATPP-FixTACA approach.

Moreover, as can be seen from Figs. 6a and 6b, compared with the other two CA approaches, the proposed ATPP-FixTACA approach does not make the actuators reach the saturation value, and hence significantly reduces the saturation duration of the actuators (refer to Fig. 3c), which can protect the actuators in the actual space mission. This is because the proposed ATPP-FixTACA approach directly considers the output saturation of the actuators when designing the adaptive law. In addition, although the other two CA approaches can use the saturation function directly to limit the actuator output, this operation cannot explain the stability, resulting in easily causing CA failure and large CA error.

Finally, it is clear from Fig. 7a that the final convergence accuracy of the allocation error of the proposed ATPP-FixTACA approach is worse than that of the other two CA approaches. This is due to the proposed ATPP-FixTACA approach directly considers the actuator saturation in the CA problem (4), focusing on the barrier-function-based ACA error $\boldsymbol{e} = (\partial L/\partial \boldsymbol{\tau})$ in Eq. (12), but not on the CA error $\|\boldsymbol{u} - \boldsymbol{D}\boldsymbol{\tau}\| = 0$. However, because we take a smaller weight matrix $\boldsymbol{M}$ and a smaller value of the weight $P$, the CA error $\|\boldsymbol{u} - \boldsymbol{D}\boldsymbol{\tau}\| = 0$ of the ATPP-FixTACA can converge to a small region close to zero. Because the proposed ATPP-FixTACA approach is based on the ATPP function, it ensures the transient and steady-state performance of the CA error $\|\boldsymbol{u} - \boldsymbol{D}\boldsymbol{\tau}\| = 0$ and reduces fluctuation of

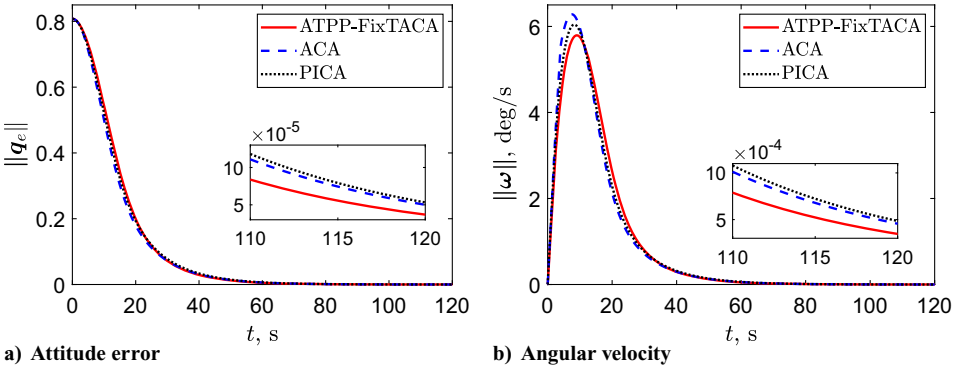


a) Attitude error b) Angular velocity

**Fig. 5 Comparison of time history of spacecraft states of three CA approaches.**

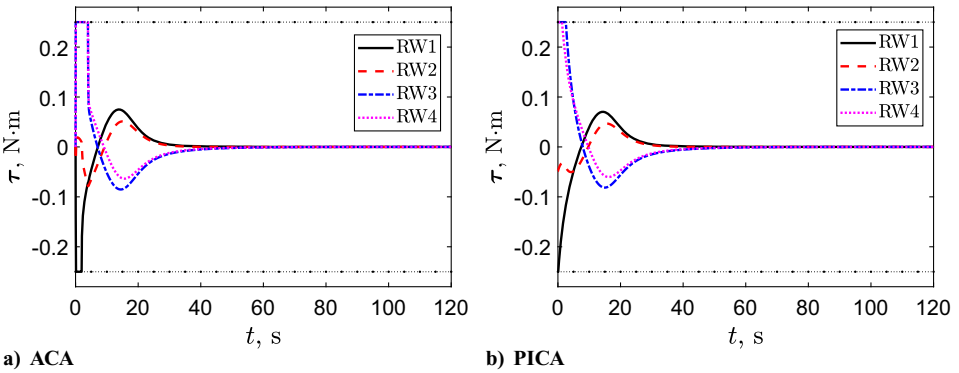


a) ACA b) PICA

**Fig. 6 Comparison of time history of reaction wheel output $\tau$ under ACA and static PICA approaches.**

the transient response, so the transient performance and convergence speed are greatly improved. We also use $\int_0^t \|\boldsymbol{u}_{\text{act}}\| \, \mathrm{d}t$ to evaluate the energy consumption of the three CA approaches, where $\boldsymbol{u}_{\text{act}} = \boldsymbol{D\tau}$ is the actual output of the actuators and $t$ is the simulation time. As observed in Fig. 7b, it is obvious that the proposed ATPP-FixTACA approach consumes the least energy among all three CA approaches.

### C. Different Parameters Comparison

In this subsection, the effects of different parameters in the ATPP-FixTACA approach are examined by numerical simulation, and the numerical simulation results are given based on scenario 1 as the above subsection. Specifically, the high-level controller is the same as the previous two subsections, and the effects of key parameters $k_1, k_2$, and $\gamma$ and weight $\boldsymbol{P}$ on ATPP-FixTACA are discussed, respectively. We consider the same attitude control problem as in Sec. VI.A, but different key parameters are selected.

#### 1. *Effect of Parameters $k_1$ and $k_2$ on ATPP-FixTACA*

Three sets of values of $k_1$ and $k_2$ are simulated for comparison, i.e., $k_1 = k_2 = 1$, $k_1 = k_2 = 5$, and $k_1 = k_2 = 45$, while other parameters remain the same. The reach times $T_{\text{reach}}$ of the three sets of parameters are 325.1385, 65.0277, and 7.2253 s, which are greater than the appointed time $T_f = 5$s.

As shown in Figs. 8a and 8b, the convergence rate of the attitude error $\|\boldsymbol{q}_e\|$ and the angular velocity $\|\boldsymbol{\omega}\|$ of spacecraft increases as $k_1$ and $k_2$ become bigger. Meanwhile, it can be seen from Fig. 8c that the larger the $k_1$ and $k_2$, the faster the convergence of the CA error $\|\boldsymbol{u} - \boldsymbol{D\tau}\|$.

In addition, as can be seen from Fig. 9, although the three sets of values of parameters $k_1$ and $k_2$ meet the output limit of the actuators and do not reach the saturation value, the excessive $k_1$ and $k_2$ cause an oscillation when the actuator output is close to its saturation value. At the same time, it is noted that with the increase of $k_1$ and $k_2$, the maximal value of the output of actuator is closer to the saturation value. Moreover, from Eq. (28), when larger $k_1$ and $k_2$ are selected, the fixed convergence time $T_{\text{reach}}$ will be reduced; i.e., the CA error has a faster convergence rate to the first-order optimal set $\mathcal{Z}$. Therefore, the parameters $k_1$ and $k_2$ can adjust the convergence rate of the CA error and the proximity of the output of the actuator to the saturation value. However, selecting an excessive $k_1$ and $k_2$ may cause oscillation of the actuators.

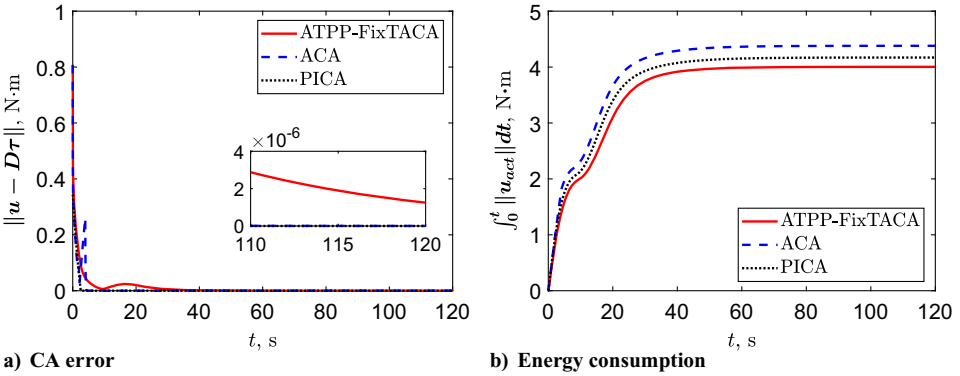


a) CA error b) Energy consumption

**Fig. 7 Comparison of time history of control allocation error and energy consumption of three ACA approaches.**

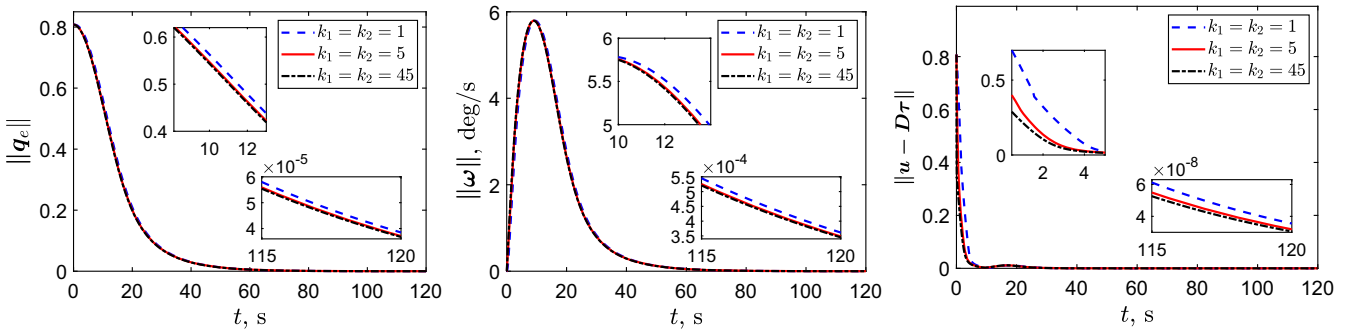


a) Attitude error b) Angular velocity c) CA error

**Fig. 8 Comparison of time history of spacecraft states and control allocation error of different $k_1$ and $k_2$ in ATPP-FixTACA.**

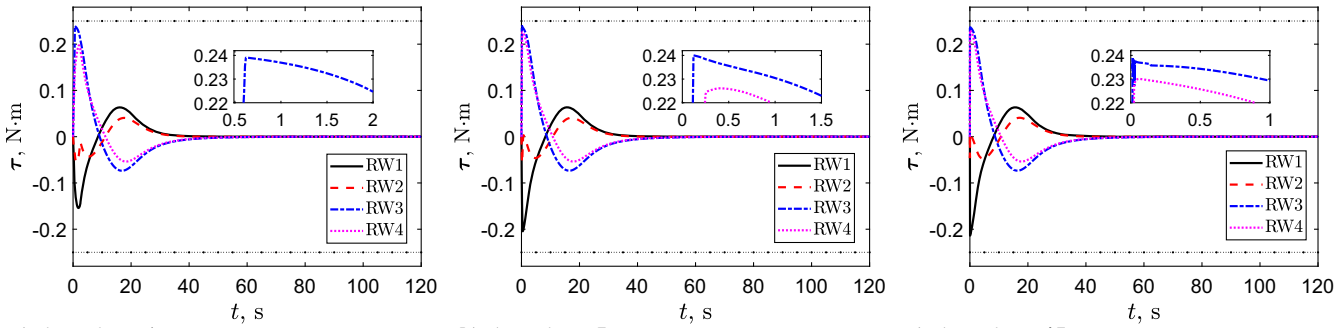


**a)** $k_1 = k_2 = 1$ **b)** $k_1 = k_2 = 5$ **c)** $k_1 = k_2 = 45$

**Fig. 9 Comparison of time history of reaction wheel output $\tau$ of different $k_1$ and $k_2$ in ATPP-FixTACA.**

*2. Effect of Parameter $\gamma$ on ATPP-FixTACA*

On the basis of Sec. VI.A, $\gamma = 0.4$, $\gamma = 0.6$, and $\gamma = 0.8$ are simulated for comparison. The reach times $T_{\text{reach}}$ of the three sets of parameters are 31.2420, 32.5138, and 48.5241 s, which are greater than the appointed time $T_f = 5$ s.

As shown in Figs. 10a and 10b, the convergence rate of the attitude error $\|\boldsymbol{q}_e\|$ and the angular velocity $\|\boldsymbol{\omega}\|$ of spacecraft is accelerated with the decrease of $\gamma$. Meanwhile, it can be seen from Fig. 10c that the smaller the $\gamma$, the faster the convergence of the CA error $\|\boldsymbol{u} - \boldsymbol{D\tau}\|$.

In addition, as can be seen from Fig. 11, although the three sets of parameters $\gamma$ meet the output limit of the actuators and do not reach the saturation value, a too small $\gamma$ causes an oscillation when the actuator approaches the saturation value. According to Eq. (28), when a smaller $\gamma$ is selected, the fixed convergence time $T_{\text{reach}}$ will be reduced, and the CA error converges faster to the CA first-order optimal set $\mathcal{Z}$. Therefore, the parameter $\gamma$ can control the convergence rate of the CA error. However, selecting a too small $\gamma$ may cause oscillation of the actuators.

*3. Effect of Parameter P on ATPP-FixTACA*

On the basis of Sec. VI.A, $P = 0.0006$, $P = 0.002$, and $P = 0.006$ are simulated for comparison. The reach times $T_{\text{reach}}$ of the three sets of parameters are 88.2401, 32.5138, and 7.2152 s, which are greater than the appointed-time $T_f = 5$ s.

As shown in Figs. 12a and 12b, the convergence rate of the attitude error $\|\boldsymbol{q}_e\|$ and the angular velocity $\|\boldsymbol{\omega}\|$ of spacecraft slows down with the increase of $P$. A smaller $P$ can be selected to decrease the state convergence error of the spacecraft. Meanwhile, it can be seen from Fig. 12c that the smaller the $P$, the faster the convergence and the better the convergence accuracy of the CA error $\|\boldsymbol{u} - \boldsymbol{D\tau}\|$.

In addition, as can be seen from Fig. 13, the actuator outputs under three sets of parameter $P$ meet the limit and do not reach the saturation value. However, choosing a small $P$ may cause oscillation when the actuator output is approaching its saturation value. At the same time, as $P$ decreases, the maximal output of the actuator is closer to its saturation value. In view of Eqs. (9) and (12), under the same conditions, a smaller $P$ leads to a smaller proportion of barrier terms in Eqs. (9) and (12), resulting in an improvement of the convergence

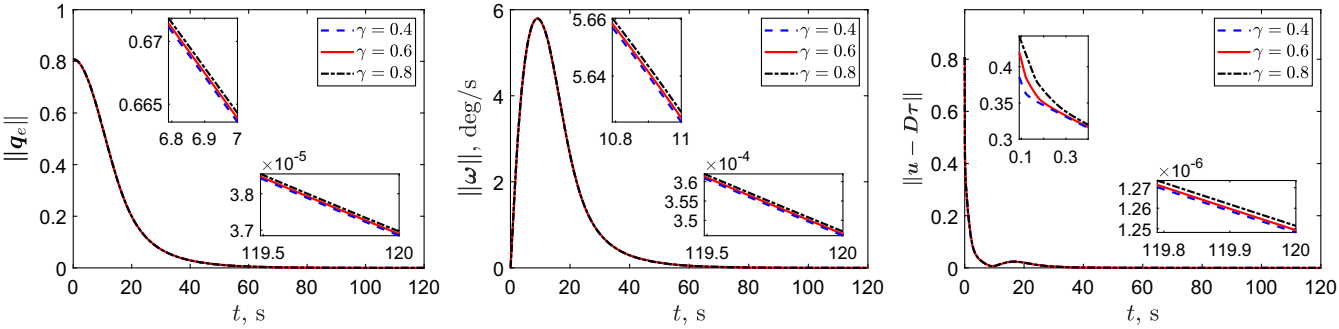


**a) Attitude error** **b) Angular velocity** **c) CA error**

**Fig. 10 Comparison of time history of spacecraft states and control allocation error of different $\gamma$ in ATPP-FixTACA.**

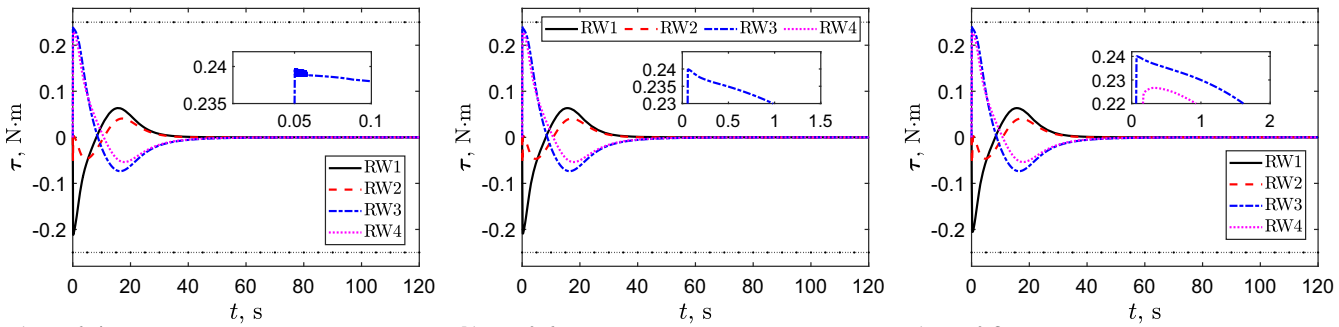


**a)** $\gamma = 0.4$ **b)** $\gamma = 0.6$ **c)** $\gamma = 0.8$

**Fig. 11 Comparison of time history of reaction wheel output $\tau$ of different $\gamma$ in ATPP-FixTACA.**

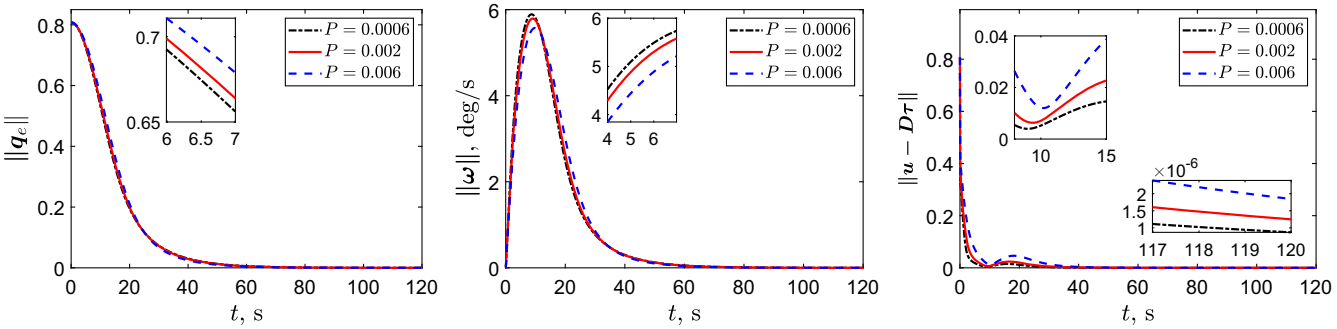


**Fig. 12 Comparison of time history of spacecraft states and control allocation error of different $P$ in ATPP-FixTACA.**

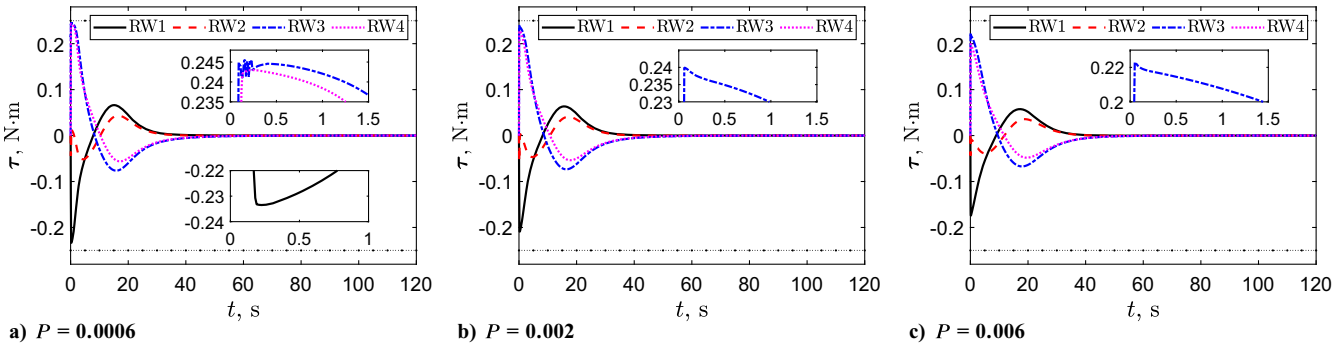


**Fig. 13 Comparison of time history of reaction wheel output $\tau$ of different $P$ in ATPP-FixTACA.**

speed and convergence accuracy of the CA error. Therefore, the parameter $P$ can control the convergence rate, the convergence accuracy of the CA error, and the proximity of the output of the actuator to the saturation value. However, choosing a too small $P$ may cause oscillation of the actuators, as observed in Fig. 13a.

## VII. Conclusions

In this paper, an adaptive CA approach taking into account the fixed-time convergence and prescribed performance of CA error is proposed for rest-to-rest attitude maneuver of overactuated spacecraft subject to actuators output constraint. First, the constrained CA problem is transformed to a barrier-function-based unconstrained CA problem. Then, an appointed-time prescribed performance-based fixed-time adaptive CA approach is developed to distribute the desired virtual control torque from the high-level controller to each actuator dynamically under conditions of satisfying the saturation limitation and the transient and steady-state constraint predefined by appointed-time prescribed performance functions. Finally, simulation results demonstrate the efficiency of the proposed appointed-time prescribed performance-based fixed-time adaptive CA approach. In future works, we will take the situation that the initial CA error does not meet the appointed-time prescribed performance function into account in the adaptive CA design.

## Acknowledgments

This work was supported in part by the National Natural Science Foundation of China (Grant Nos. 62103275, U20B2054, and U20B2056), the Natural Science Foundation of Shanghai (No. 20ZR1427000), and the Shanghai Sailing Program (No. 20YF1421600). The support provided by China Scholarship Council during a visit of Zeyu Kang to University of Toronto is acknowledged (No. 202106230180).

## References

[1] Johansen, T. A., and Fossen, T. I., "Control Allocation—A Survey," *Automatica*, Vol. 49, No. 5, 2013, pp. 1087–1103. https://doi.org/10.1016/j.automatica.2013.01.035

[2] Fossen, T. I., and Johansen, T. A., "A Survey of Control Allocation Methods for Ships and Underwater Vehicles," *2006 14th Mediterranean Conference on Control and Automation*, Inst. of Electrical and Electronics Engineers, New York, 2006, pp. 1–6. https://doi.org/10.1109/MED.2006.328749

[3] Benosman, M., Liao, F., Lum, K. Y., and Wang, J. L., "Nonlinear Control Allocation for Non-Minimum Phase Systems," *IEEE Transactions on Control Systems Technology*, Vol. 17, No. 2, 2009, pp. 394–404. https://doi.org/10.1109/TCST.2008.924568

[4] Alwi, H., and Edwards, C., "Fault Tolerant Control using Sliding Modes with Online Control Allocation," *Automatica*, Vol. 44, No. 7, 2008, pp. 1859–1866. https://doi.org/10.1016/j.automatica.2007.10.034

[5] Shen, Q., Wang, D. W., Zhu, S. Q., and Poh, E. K., "Inertia-Free Fault-Tolerant Spacecraft Attitude Tracking Using Control Allocation," *Automatica*, Vol. 62, Dec. 2015, pp. 114–121. https://doi.org/10.1016/j.automatica.2015.09.027

[6] Tjønnås, J., and Johansen, T. A., "Adaptive Control Allocation," *Automatica*, Vol. 44, No. 11, 2008, pp. 2754–2765. https://doi.org/10.1016/j.automatica.2008.03.031

[7] Chen, Y., and Wang, J. M., "Adaptive Energy-Efficient Control Allocation for Planar Motion Control of Over-Actuated Electric Ground Vehicles," *IEEE Transactions on Control Systems Technology*, Vol. 22, No. 4, 2014, pp. 1362–1373. https://doi.org/10.1109/TCST.2013.2287560

[8] Hu, Q. L., and Tan, X., "Dynamic Near-Optimal Control Allocation for Spacecraft Attitude Control Using a Hybrid Configuration of Actuators," *IEEE Transactions on Aerospace and Electronic Systems*, Vol. 56, No. 2, 2020, pp. 1430–1443. https://doi.org/10.1109/TAES.2019.2934697

[9] Kang, Z. Y., Shen, Q., and Wu, S. F., "Constrained Attitude Control of Over-Actuated Spacecraft Subject to Instrument Pointing Direction Deviation," *IEEE Control Systems Letters*, Vol. 5, No. 6, 2021, pp. 1958–1963. https://doi.org/10.1109/LCSYS.2020.3044984

[10] Liao, F., Lum, K. Y., Wang, J. L., and Benosman, M., "Constrained Nonlinear Finite-Time Control Allocation," *2007 American Control Conference*, Inst. of Electrical and Electronics Engineers, New York, 2007, pp. 3801–3806. https://doi.org/10.1109/ACC.2007.4282512

[11] Sidi, M. J., *Spacecraft Dynamics and Control: A Practical Engineering Approach*, Vol. 7, Cambridge Univ. Press, Cambridge, England, U.K., 1997, Chap. 4, pp. 88–111.

[12] Thakur, D., Srikant, S., and Akella, M. R., "Adaptive Attitude-Tracking Control of Spacecraft with Uncertain Time-Varying Inertia Parameters," *Journal of Guidance, Control, and Dynamics*, Vol. 38, No. 1, 2015, pp. 41–52. https://doi.org/10.2514/1.G000457

[13] Polyakov, A., "Nonlinear Feedback Design for Fixed-Time Stabilization of Linear Control Systems," *IEEE Transactions on Automatic Control*, Vol. 57, No. 8, 2012, pp. 2106–2110. https://doi.org/10.1109/TAC.2011.2179869

[14] Wang, H. Q., Bai, W., Zhao, X. D., and Liu, P. X. P., "Finite-Time-Prescribed Performance-Based Adaptive Fuzzy Control for Strict-Feedback Nonlinear Systems with Dynamic Uncertainty and Actuator Faults," *IEEE Transactions on Cybernetics*, Vol. 52, No. 7, 2021, pp. 1–13. https://doi.org/10.1109/TCYB.2020.3046316

[15] Lu, K. F., and Xia, Y. Q., "Adaptive Attitude Tracking Control for Rigid Spacecraft with Finite-Time Convergence," *Automatica*, Vol. 49, No. 12, 2013, pp. 3591–3599. https://doi.org/10.1016/j.automatica.2013.09.001

[16] Sun, Y. M., Chen, B., Lin, C., and Wang, H. H., "Finite-Time Adaptive Control for a Class of Nonlinear Systems with Nonstrict Feedback Structure," *IEEE Transactions on Cybernetics*, Vol. 48, No. 10, 2018, pp. 2774–2782. https://doi.org/10.1109/TCYB.2017.2749511

[17] Kristiansen, R., Nicklasson, P. J., and Gravdahl, J. T., "Spacecraft Coordination Control in 6-DOF: Integrator Backstepping vs Passivity-Based Control," *Automatica*, Vol. 44, No. 11, 2008, pp. 2896–2901. https://doi.org/10.1016/j.automatica.2008.04.019

[18] Wang, H. Q., Liu, P. X. P., Niu, B., Zhao, X. D., and Liu, X. P., "Adaptive Fuzzy Finite-Time Control of Nonlinear Systems with Actuator Faults," *IEEE Transactions on Cybernetics*, Vol. 50, No. 5, 2020, pp. 1786–1797. https://doi.org/10.1109/TCYB.2019.2902868

[19] Angelis, E. L. D., Giulietti, F., Ruiter, A. H. J. D., and Avanzini, G., "Spacecraft Attitude Control Using Magnetic and Mechanical Actuation," *Journal of Guidance, Control, and Dynamics*, Vol. 39, No. 3, 2016, pp. 564–573. https://doi.org/10.2514/1.G000957

[20] Luo, W. C., Chu, Y. C., and Ling, K. V., "Inverse Optimal Adaptive Control for Attitude Tracking of Spacecraft," *IEEE Transactions on Automatic Control*, Vol. 50, No. 11, 2005, pp. 1639–1654. https://doi.org/10.1109/TAC.2005.858694

[21] Dong, L., Yan, J., Yuan, X., He, H. B., and Sun, C. Y., "Functional Nonlinear Model Predictive Control Based on Adaptive Dynamic Programming," *IEEE Transactions on Cybernetics*, Vol. 49, No. 12, 2019, pp. 4206–4218. https://doi.org/10.1109/TCYB.2018.2859801

[22] Shen, Q., Wang, D. W., Zhu, S. Q., and Poh, E. K., "Integral-Type Sliding Mode Fault-Tolerant Control for Attitude Stabilization of Spacecraft," *IEEE Transactions on Control Systems Technology*, Vol. 23, No. 3, 2015, pp. 1131–1138. https://doi.org/10.1109/TCST.2014.2354260

[23] Jorge, N., and Stephen, J. W., *Numerical Optimization*, Springer, Berlin, 2006, Chap. 19.1, pp. 564–566.

[24] Gazi, V., "Swarm Aggregations Using Artificial Potentials and Sliding-Mode Control," *IEEE Transactions on Robotics*, Vol. 21, No. 6, 2005, pp. 1208–1214. https://doi.org/10.1109/TRO.2005.853487

[25] Levant, A., "Higher-Order Sliding Modes, Differentiation and Output-Feedback Control," *International Journal of Control*, Vol. 76, Nos. 9–10, 2003, pp. 924–941. https://doi.org/10.1080/0020717031000099029

[26] Zou, A.-M., Hou, Z.-G., and Tan, M., "Adaptive Control of a Class of Nonlinear Pure-Feedback Systems using Fuzzy Backstepping Approach," *IEEE Transactions on Fuzzy Systems*, Vol. 16, No. 4, 2008, pp. 886–897. https://doi.org/10.1109/TFUZZ.2008.917301